

Biogeochemistry of an Iron-Rich Hypersaline Microbial Mat (Camargue, France)

A. Wieland¹, J. Zopfi², M. Benthien¹ and M. Kühl¹

(1) Marine Biological Laboratory, University of Copenhagen, Strandpromenaden 5, DK-3000 Helsingør, Denmark

(2) Danish Center for Earth System Science, University of Southern Denmark, Campusvej 55, DK-5230 Odense M, Denmark

Received: 7 August 2003 / Accepted: 30 October 2003 / Online publication: 21 December 2004

Abstract

In situ microsensor measurements were combined with biogeochemical methods to determine oxygen, sulfur, and carbon cycling in microbial mats growing in a solar saltern (Salin-de-Giraud, France). Sulfate reduction rates closely followed the daily temperature changes and were highest during the day at 25°C and lowest during the night at 11°C, most probably fueled by direct substrate interactions between cyanobacteria and sulfate-reducing bacteria. Sulfate reduction was the major mineralization process during the night and the contribution of aerobic respiration to nighttime DIC production decreased. This decrease of aerobic respiration led to an increasing contribution of sulfide (and iron) oxidation to nighttime O₂ consumption. A peak of elemental sulfur in a layer of high sulfate reduction at low sulfide concentration underneath the oxic zone indicated anoxygenic photosynthesis and/or sulfide oxidation by iron, which strongly contributed to sulfide consumption. We found a significant internal carbon cycling in the mat, and sulfate reduction directly supplied DIC for photosynthesis. The mats were characterized by a high iron content of 56 μmol Fe cm⁻³, and iron cycling strongly controlled the sulfur cycle in the mat. This included sulfide precipitation resulting in high FeS contents with depth, and reactions of iron oxides with sulfide, especially after sunset, leading to a pronounced gap between oxygen and sulfide gradients and an unusual persistence of a pH peak in the uppermost mat layer until midnight.

Introduction

Hypersaline environments supporting extensive growth of cyanobacterial mats include natural shallow coastal areas (e.g., [25, 33, 48]) and man-made solar salterns (e.g., [5, 7, 8, 42]). Solar salterns generally consist of a series of shallow ponds with progressively increasing salinity due to evaporation. Thick and cohesive microbial mats dominated by the filamentous cyanobacterium *Microcoleus chthonoplastes* are found in ponds with salinities ranging from ~60 to 120‰ [7, 41].

Hypersaline microbial mats are characterized by closely coupled biogeochemical cycles of O₂, sulfur and carbon [3, 57]. Due to the close proximity of the different groups of mat-inhabiting microorganisms and the small vertical scale of the active layer, different processes closely interact, leading to efficient turnover of major electron acceptors/donors in the upper few millimeters of microbial mats (reviewed in [50]). Dissimilatory sulfate reduction, the dominant process of anaerobic carbon mineralization in hypersaline microbial mats, occurs in all mat layers, even in the highly oxygenated surface layer [2, 17, 27]. However, the produced sulfide only accumulates just underneath the oxic zone due to rapid sulfide oxidation in the uppermost mat layer in the presence of oxygen. Thus, the anoxic zone is in general completely represented by the sulfidic zone and a sharp transition between the oxic and the sulfidic zone occurs in hypersaline microbial mats as a narrow zone of overlapping O₂ and sulfide gradients [28, 46, 57].

In this study, the biogeochemistry of iron-rich hypersaline cyanobacterial mats from a pre-concentration pond of the Salin-de-Giraud saltern, Camargue, France, is described. *In situ* microsensor measurements (O₂, H₂S, pH) were performed over a diel cycle and combined with biogeochemical methods for determination of sulfate reduction rates, pools of iron, and oxidized sulfur intermediates. Iron-rich microbial mats composed of phototrophs or iron bacteria have previously been found

Present address of J. Zopfi: Laboratoire de Microbiologie, Institut de botanique, Université de Neuchâtel, Emile Argand 9, CH-2007 Neuchâtel, Switzerland

Correspondence to: A. Wieland; E-mail: awieland@zi.ku.dk

in freshwater and some marine settings such as hydrothermal vent systems [4, 9, 11, 12, 31, 43]. To our knowledge, this study is the first biogeochemical study of an iron-rich hypersaline microbial mat system.

Materials and Methods

Microsensor Measurements of O_2 , pH, and H_2S Depth Profiles. Clark-type O_2 [44] and H_2S microsensors [35] connected to a picoammeter (UniSense A/S, Denmark), and a glass pH microelectrode [45] connected to a high-impedance mV-meter (MasCom, Germany) were fixed together and operated via a motorized micromanipulator (Märzhäuser, Germany; Oriel, USA) mounted on a heavy solid stand. Microsensor signals were recorded with strip chart recorders (Servogor, UK) and a computer data acquisition system (LabView, National Instruments, USA). Measurements were done *in situ* from a small measuring platform placed in a shallow pre-concentration pond of the Salin-de-Giraud saltern, France. All electronic instruments were operated via batteries.

The O_2 microsensor had a tip diameter of 8 μm , a stirring sensitivity of $\sim 0\%$, and a response time, t_{90} , of ~ 0.3 s. The H_2S microsensor had a tip diameter of 15 μm and was coated with a black enamel paint to avoid light interference [35], and additionally with a white enamel paint to avoid heating of the sensor when exposed to sunlight. The pH-sensitive tip of the pH microelectrode was 150 μm long and 20 μm in diameter.

The O_2 microsensor was linearly calibrated on site from readings of microsensor current in the overlying water and in the anoxic part of the mat (0% O_2). Dissolved O_2 concentrations in the overlying water were determined by Winkler titration [21]. The H_2S and the pH microelectrodes were calibrated in the laboratory of the salt company at Salin-de-Giraud prior to the *in situ* measurements. The pH microelectrode was calibrated in standard buffer solutions (Radiometer, Denmark). During the diel cycle, the pH of the overlying water was regularly determined with a pH meter (Radiometer, Denmark) calibrated in the same buffer solutions. The reading of the pH microelectrode in the overlying water was adjusted to the measured pH of the water. After the field experiment, the pH microelectrode was calibrated in the laboratory (Marine Biological Laboratory, University of Copenhagen) as a function of temperature to correct for the effect of temperature variations during *in situ* measurements. The H_2S microsensor was calibrated in anoxic buffer solution (0.2 M phosphate buffer, pH 7.5) by adding increasing amounts of a sulfide stock solution of known concentration. Microsensor signals were recorded after each addition when stable readings were reached. Calculation of dissolved hydrogen sulfide (H_2S) and total sulfide (H_2S_{tot}) concentration from H_2S

and pH microsensor data were done according to Wieland and Kühl [57], using pK_1 values calculated from *in situ* temperatures [24]. In the following, total sulfide, H_2S_{tot} , denotes the sum of H_2S , HS^- , and S^{2-} concentrations.

Water salinity and temperature were measured with a refractometer (Atago, Japan) and a digital thermometer (Omnitherm, Germany). The downwelling scalar irradiance at the mat surface ($E_{0,d}$) was determined with an underwater quantum scalar irradiance meter (QSL-101, Biospherical Instruments, USA).

Oxygen fluxes were calculated from microsensor data as described in Wieland and Kühl [57]. Sulfide fluxes were calculated from the linear part of the respective total sulfide profiles using Fick's first law of diffusion, estimating mat porosity (0.9) and the sediment diffusion coefficient as described in Wieland and Kühl [57]. Sulfide fluxes represent areal net rates of sulfide production/consumption, i.e., net sulfide turnover rates in the mat. However, they do not represent a net production of sulfide by the mat, since all sulfide produced by sulfate reduction is consumed within the mat.

Determination of DIC and O_2 Fluxes from Core Incubations. Fluxes of dissolved inorganic carbon (DIC) and O_2 were determined in the afternoon (16:25 h), just before midnight (23:32 h), and in the early morning before sunrise (4:14 h), whereas flux determinations around noon were impossible because of experimental difficulties.

A Plexiglas core (52 mm i.d.) was inserted in the mats leaving an appropriate water volume above the enclosed mat surface (~ 21 cm²). For the incubations in closed chambers, a transparent lid with a mounted stirrer magnet and a port for a robust O_2 electrode [19] was put on top of the core. Before and after each incubation 10-mL water samples were transferred into screwcapped glass vials (Exetainers, Labco, UK) containing 100 μL of a saturated $HgCl_2$ solution to stop biological activity. The samples were kept cold and dark until DIC concentrations were quantified with a CO_2 analyzer (Coulometer CM5012, UIC, USA). After insertion of the O_2 electrode, the change of dissolved O_2 concentration in the chamber was recorded with a strip chart recorder (Servogor, UK). Stirring of the water during incubations was realized with a battery-driven watertight magnetic-stirrer. The lid was removed again to allow re-equilibration with the surrounding pond water after each incubation.

The flux of oxygen, J_{Ox} , was calculated as:

$$J_{Ox} = \alpha \times V \times A^{-1} \quad (1)$$

where α is the initial rate of oxygen depletion or accumulation after closing the lid, A is the mat surface area within the core, and V is the volume of the enclosed water above the mat.

The flux of inorganic carbon, J_{DIC} , was calculated as:

$$J_{\text{DIC}} = (C_t - C_0) \times V \times (A \times t)^{-1} \quad (2)$$

where t is the incubation time, and C_0 and C_t are the DIC concentrations at the start and at the end of the incubation, respectively.

Rate Measurement and 2D Mapping of Bacterial Sulfate Reduction. Triplicate mat cores (18 mm i.d.) were collected at defined times during the diel cycle in truncated 20-mL plastic syringes. Twenty-five microliters of $^{35}\text{SO}_4^{2-}$ tracer (600 kBq, salinity 100‰) were added to the uppermost centimeter of each mat core by five vertical injections. The cores were incubated for 45 min at *in situ* conditions and then immediately frozen in liquid nitrogen and finally stored at -80°C . Prior to analysis, the frozen mat cores were sliced with a razor blade at horizontal depth-intervals of ~ 1 mm. The slices were immediately transferred into tubes containing 5% ice-cooled zinc acetate and homogenized. Sulfate reduction rates were determined by the single-step chromium reduction method [15, 27].

The two-dimensional distribution of sulfate reduction was determined at high spatial resolution by incubating $^{35}\text{SO}_4^{2-}$ -labeled silver foil in the mat (Visscher PT, pers. comm.; [47, 54]). Pieces of silver foil ($25 \times 17 \times 0.1$ mm; Sigma, USA) were cleaned with acetone, rinsed with Milli-Q water, treated with 0.1 M HNO_3 for 1 min, and rinsed with Milli-Q water again. Both sides of the cleaned foils were subsequently coated with ^{35}S -labeled sulfate with a specific activity of 239 MBq mL^{-1} and 28 g L^{-1} NaCl. For this, foil pieces and tracer-soaked (60 μL) Kimwipes were stacked and left to dry in a closed Petri dish for about 24 h. With a scalpel a cut of 3 cm length and about 2 cm depth was made in a freshly sampled mat piece, and the silver foil was carefully inserted. After an incubation time of 3 to 13.5 h the foil was removed and washed five times with hypersaline water from the sampling site to remove residual $^{35}\text{SO}_4^{2-}$. The reduced sulfate, which had precipitated as Ag^{35}S on the foil surface, was then digitally mapped with a β -microimager (Biospace Mésures, France) using a scanning time of 1 h.

Determination of Iron (Fe(II)/Fe(III)) and Sulfur Intermediates (S^0 , $\text{S}_2\text{O}_3^{2-}$, SO_3^{2-}). For determination of iron and oxidized sulfur intermediates at specific times during the diel cycle, mat cores taken with truncated 5-mL plastic syringes were immediately frozen in liquid nitrogen and stored on dry ice and finally at -80°C until further processing. The upper 6–9 mm of the frozen mat cores was thin-sectioned with a cryomicrotome (Microm, Germany) at -37°C and a horizontal depth resolution of 300 μm . The frozen slices were

immediately transferred into Eppendorf tubes containing either (a) 1 mL H_2SO_4 (15.5 mM) for subsequent determination of iron and manganese, (b) 100 μL of ZnCl_2 (5%) for later S^0 determination, or (c) 100 μL of bimane reagent (16 mM mono-bromobimane in acetonitrile) and 100 μL of HEPES/EDTA buffer (160 mM/16 mM, pH 8) for the determination of thiosulfate and sulfite.

After an extraction time of 2 h, samples for iron and manganese determination were centrifuged and the supernatant was stored at 4°C until further analysis. Extracted Fe^{2+} , Fe^{3+} , and Mn^{2+} ions were separated by ion chromatography and detected at 530 nm after post-column derivatization with the metal complexing agent 4-(2-pyridylazo)resorcinol as described in detail elsewhere (Dionex Technical Note 10, method A). With this procedure, iron sulfide (FeS) and siderite (FeCO_3) were completely extracted from the mat, whereas iron oxides were probably only incompletely extracted.

Mat slices fixed for S^0 determination were frozen again until further processing. Elemental sulfur was extracted with methanol (1 mL) for about 16 h on a rotary shaker and quantified by RP-HPLC and UV-detection at 265 nm as described by Zopfi et al. [58].

After a derivatization time of 30 min, slices for thiosulfate and sulfite determination were fixed with 100 μL MESA (200 mM, methanesulfonic acid) and either kept on ice if analyzed at the same day or, alternatively, frozen again and kept at -20°C . Quantification of thiosulfate and sulfite was performed by gradient RP-HPLC and fluorescence detection as described in [58].

Total HCl extractable iron (Fe(II) + Fe(III)) in the top 6 mm of hypersaline microbial mats from our sampling site as well as from the Ebro Delta (Spain) [40] and Solar Lake (Egypt) [33] was determined by incubating the samples with 1 M HCl for 48 h, thereby extracting FeS, FeCO_3 , and poorly crystalline iron oxides [53]. Subsequently, 20–50 μL extract was added to 2.5 mL of reducing ferrozine solution (0.4 g L^{-1} ferrozine + 10 g L^{-1} hydroxylamine hydrochloride in 50 mM HEPES) and measured at 562 nm [37, 53].

Mat cores for determination of solid-phase sulfur species were collected two times during the diel cycle and were sliced and fixed as described above. Acid volatile sulfur ($\text{AVS} = \text{H}_2\text{S}_{\text{tot}} + \text{FeS}$) and chromium reducible sulfur ($\text{CRS} = \text{S}^0 + \text{FeS}_2$) were determined by a two-step distillation with 6 M HCl followed by boiling in a 1 M acidic CrCl_2 solution [15]. The liberated H_2S was collected in AgNO_3 traps and the dry weight of the Ag_2S precipitate was determined. After AVS determination, total iron (Fe(II) + Fe(III)) was determined in the extract of the HCl-acidified mat samples as described above. Fe(II) was determined by using ferrozine solution without hydroxylamine hydrochloride.

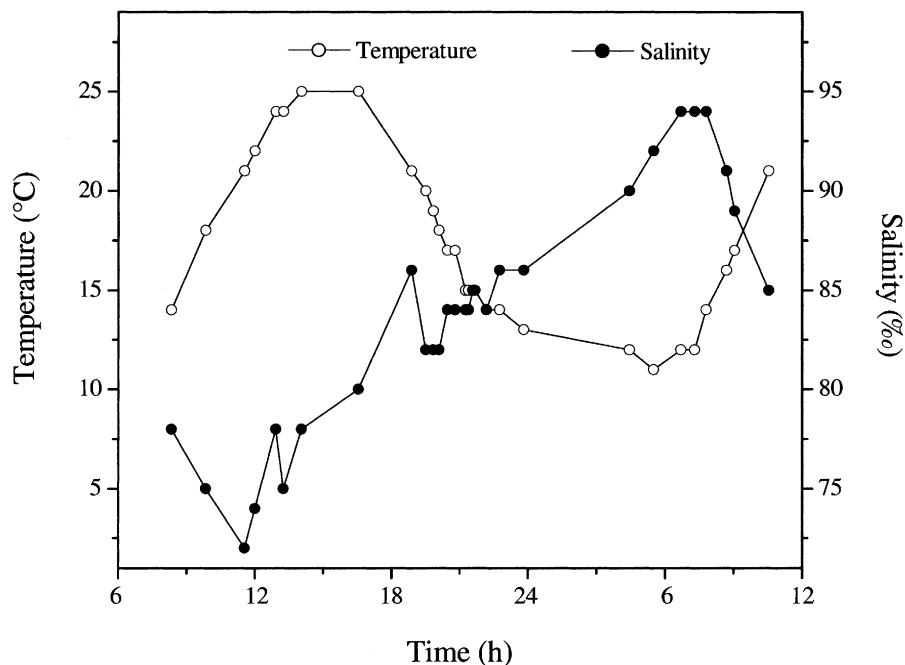


Figure 1. *In situ* variation of water temperature and salinity during a diel cycle in the pre-concentration pond of the Salin-de-Giraud solar salt works.

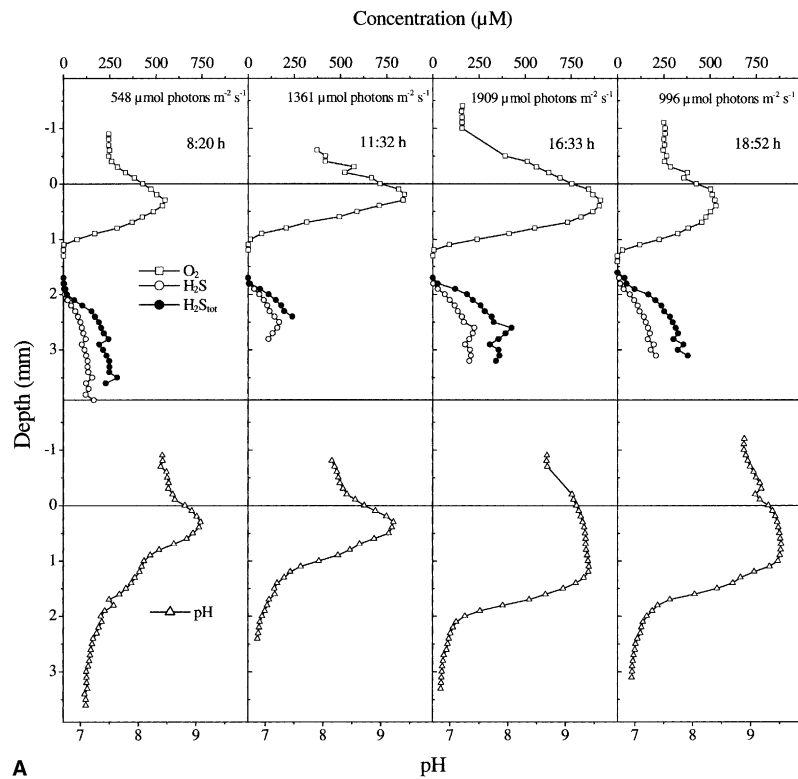
Results

Mat Structure and Composition. The hypersaline microbial mat investigated in this study covered the bottom of a pre-concentration pond in the Salin-de-Giraud solar salt works, located on the Mediterranean French coast in the Rhône Delta (Camargue, France; [7]). The water height in this pond normally does not exceed ~20 cm [16] and is influenced by water exchange with adjacent ponds, regulated by the salt company. The 5- to 8-cm-thick mat had a soft light-brownish surface and was very cohesive and finely laminated underneath. The surface layer was composed of diatoms (mainly *Nitzschia* sp.), unicellular cyanobacteria, and remnants of mosquito pupae. Below, filamentous cyanobacteria, mostly *Microcoleus chthonoplastes*, formed a distinct dark-green cohesive band. In the upper part of the mat, also white bands of filamentous sulfur-oxidizing bacteria (*Beggiatoa* sp.) and bands of rusty-brown color were observed. The detailed microbial composition and depth-zonation of major bacterial groups in the mat will be published elsewhere (A. Fourçans et al., in prep.). This analysis of mat samples taken simultaneously during the diel cycle in June 2001 showed besides the presence of different populations of sulfate-reducing (SRB) and purple anoxygenic bacteria (PAB) in the uppermost 4 mm of the mat, also diel migration patterns of some of these populations. Biomarker, microscopic, and molecular analyses of mats taken in 2000 and spectral scalar irradiance measurements with fiber-optic microprobes in mats taken in February 2001 revealed the presence of different populations of cyanobacteria (mainly *M. chthonoplastes*),

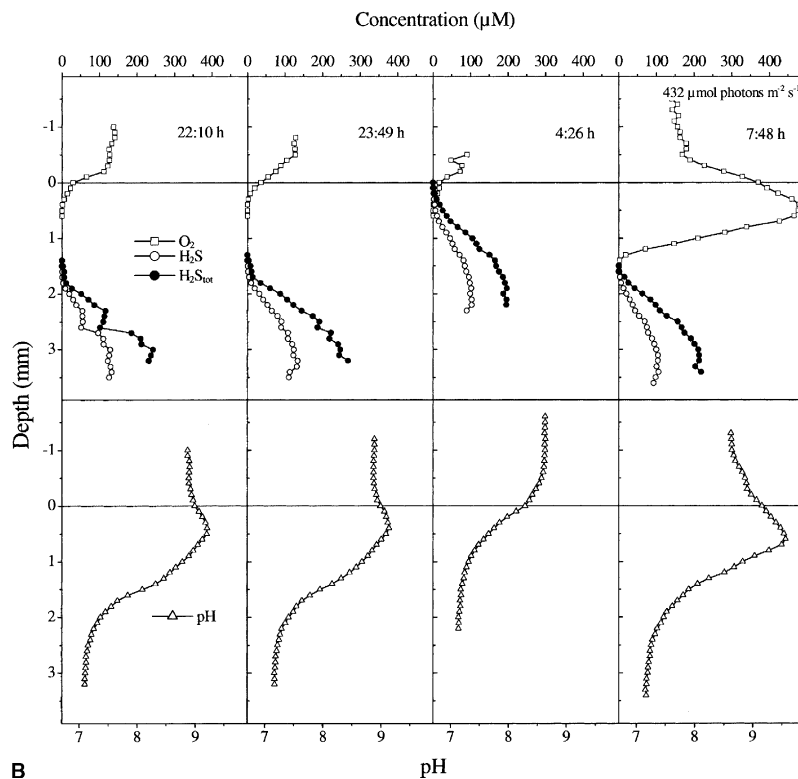
SRB (e.g., *Desulfovibrio* sp., *Desulfobacter* sp.), PAB (e.g. *Halochromatium salexigens*, *Roseospira marina*, *Rhodobacter* sp., *Ectothiorhodospira* sp.), and green *Chloroflexus*-like bacteria [16]. The reduced mat layers at greater depths had a salient metallic black appearance. However, after air exposure and subsequent oxidation, alternating green and brown bands composed of buried *Microcoleus*- and iron-rich layers became visible.

Diel Variation of Environmental Parameters and Microgradients. A pronounced diel variation of both water temperature and salinity was found (Fig. 1). Water temperature was highest in the afternoon (25°C) and lowest in the early morning (11°C). After an initial drop, salinity strongly increased from 72 to 94‰ and decreased again in the early morning of the second day. Such pronounced variations were mainly caused by water exchange with adjacent ponds. During the first day of measurements, strong winds prevailed in the morning and afternoon causing an elevated water level in the pond. Because of sluice opening by the company, the water level then dropped significantly during the night, leading to a change of the water flow.

Oxygen concentration within the mat increased during the day until the afternoon (16:33 h) and then decreased with decreasing irradiance (Fig. 2A, upper panel). During the first day of measurements, O₂ penetration was highest in the afternoon and early evening after cessation of the wind. At irradiances <50 μmol photons m⁻² s⁻¹ (after 21:00 h), O₂ penetration gradually decreased (profiles not shown) to 0.4 mm during the night (Fig. 2B, upper panel). In the morning of the sec-



A



B

Figure 2. *In situ* depth profiles of O_2 , pH, H_2S , and total sulfide (H_2S_{tot}) at specific times during the diel cycle. (A) Profiles during daytime and (B) during nighttime and morning of the second day of the diel cycle. Note different scales.

ond day, O_2 penetration was highest and the oxic zone was confined to the top 1.5 mm of the mat.

During daytime, the upper sulfide boundary was located at 1.7 mm depth (8:20–16:33 h), and maximal

sulfide concentrations and the steepness of the sulfide gradients only slightly increased. The oxic and the sulfidic zones were separated by a zone of 0.4–0.6 mm (Fig. 2A). The pH increased in the uppermost part of the mat due

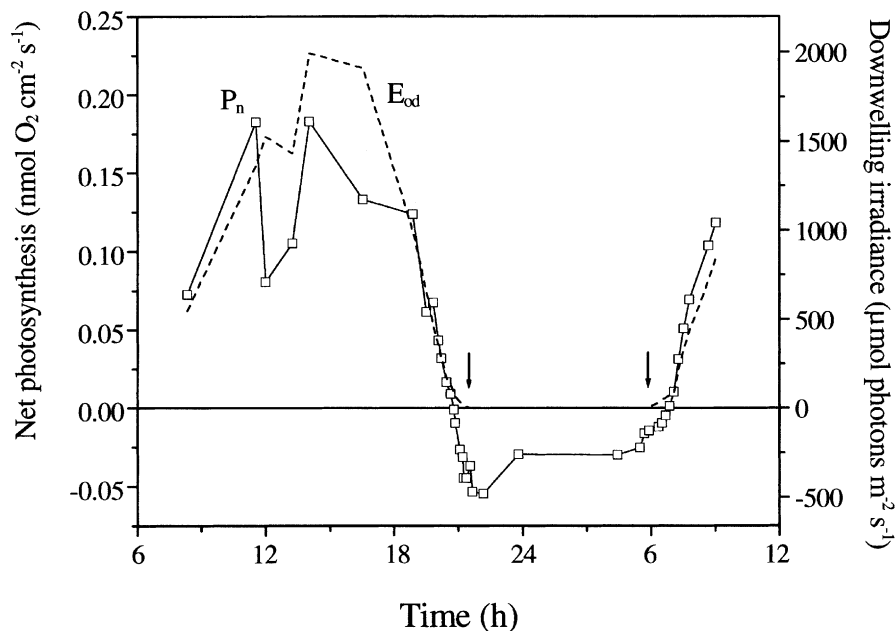


Figure 3. *In situ* areal rates of net photosynthesis (P_n) in the Camargue microbial mat over a diel cycle. The dotted line shows the downwelling scalar irradiance at the mat surface (E_{od}).

to photosynthetic CO_2 fixation (Fig. 2A, lower panel). Below this peak, pH decreased again due to respiration, sulfide oxidation and fermentation in the different zones of the mat. Both the peak of pH and the zone of elevated pH increased during the day, reaching maximum values of pH 9.5 in the evening.

After sunset, when both oxygenic and anoxygenic photosynthesis ceased, O_2 concentration and penetration rapidly decreased (Fig. 2B, upper panel). The upper sulfide boundary, however, did not move significantly upward until midnight, resulting in an increased gap between the lower O_2 and the upper sulfide boundary of ~ 1 mm. During this period of ~ 2 – 3 h of darkness, an atypical peak of pH (pH 9.1–9.2) persisted in the uppermost mat layer (Fig. 2B, lower panel), which was obviously not related to photosynthetic activity. Before sunrise (4:26 h), pH finally strongly decreased in the uppermost mat layers, as often found in dark-incubated hypersaline microbial mats [46, 57]. At this time, sulfide was also detectable in the uppermost mat layers, resulting in a narrow zone of O_2 and sulfide overlap. After sunrise and onset of photosynthesis, O_2 concentration and penetration depth, the depth of the upper sulfide boundary and the pH in the uppermost mat layer increased again.

Diel Variation of O_2 Fluxes. The O_2 flux across the mat–water interface, representing areal rates of net photosynthesis (P_n), covaried with the incident irradiance (Fig. 3). At $91 \mu\text{mol photons m}^{-2} \text{s}^{-1}$ (20:48 h), the mat turned from net O_2 production to a net O_2 uptake. At low irradiances during sunset, O_2 consumption rates ($-P_n$) initially increased and decreased then to a lower rate of dark O_2 consumption during the night. At sunrise,

net photosynthesis gradually increased again and a net O_2 production was detected at an irradiance of $71 \mu\text{mol photons m}^{-2} \text{s}^{-1}$ (6:52 h).

Diel Variation and 2D Distribution of Sulfate Reduction Rates. Sulfate reduction rates were significantly higher during the day than during the night (Fig. 4). At all times, sulfate reduction rates (SRR) were highest in the top 5 mm of the mat and showed a clear maximum below 1 mm depth. Also by two-dimensional mapping of SRR with the silver foil technique, a clear zonation of maximal SRR underneath the surface was found (Fig. 5). Maximal sulfate reduction activity was, however, detected at greater depths (~ 4 – 6 mm depth). A clear horizontal lamination pattern of SRR within the upper 16 mm and the occurrence of local zones of increased SRR were revealed by this technique. Both sides of the silver foil showed a similar pattern of alternating mat layers of high and low activity with depth (Fig. 5, right).

Areal rates of sulfate reduction (aSRR), obtained by depth-integration of the data shown in Fig. 4, increased in the morning to maximal rates at noon and then decreased again in the early evening, following the diel temperature oscillation (Fig. 6a). Maximal rates during the day were >6 times higher than minimal rates during the night. The aSRR showed a linear correlation with the covarying daily temperature and E_{od} changes ($R = 0.94$ and 0.97), but not with the depth-integrated O_2 concentration in the mat ($R = 0.57$, data not shown).

The apparent temperature dependence of sulfate reduction was expressed by a high activation energy of 99 kJ mol^{-1} and a resulting Q_{10} of 4 over the temperature range from 15 to 25°C (Fig. 6b). Although the sulfide

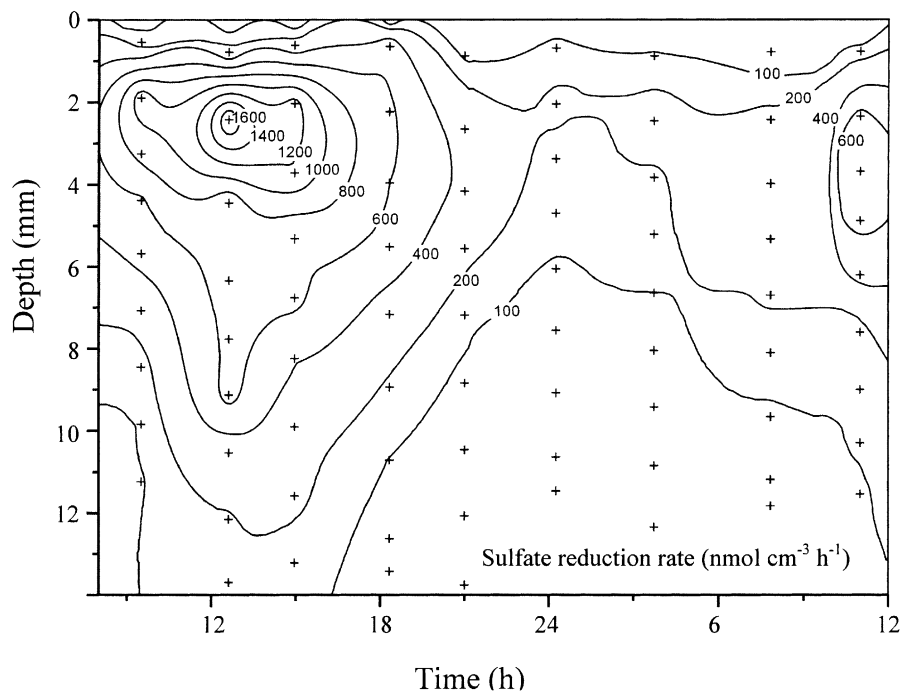


Figure 4. Isopleths of *in situ* volumetric sulfate reduction rates (SRR) in the Camargue microbial mats. Each cross represents the mean of triplicate SRR measurements.

fluxes ($J_{H_2S_{tot}}$) calculated from the microprofiles (Fig. 2) showed a similar pattern to the aSRR, the difference between both rates varied strongly during the diel cycle (Fig. 6a). Calculated sulfide fluxes ($J_{H_2S_{tot}}$) are measures of net rates of sulfide production below the variable depth in the mat where production exceeds consumption, whereas aSRR represent gross rates of sulfide pro-

duction. A difference between gross and net sulfide production rates can result from diverse sulfide removal mechanisms. These include biological and chemical sulfide oxidation in the oxic layer, anaerobic oxidation by anoxygenic photosynthesis, polysulfide formation, and oxidation by iron and manganese oxides, as well as FeS precipitation.

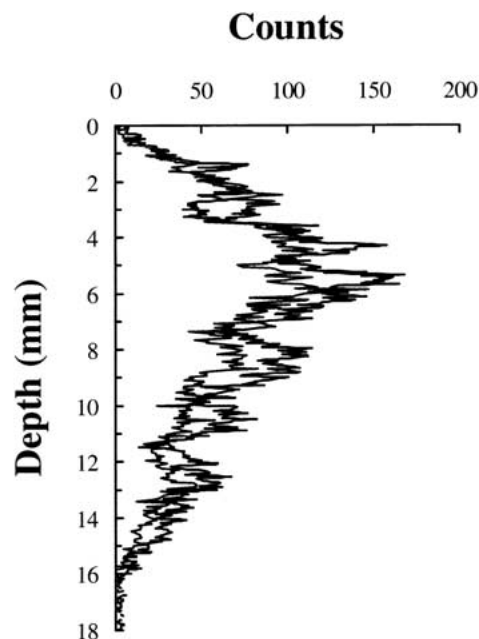
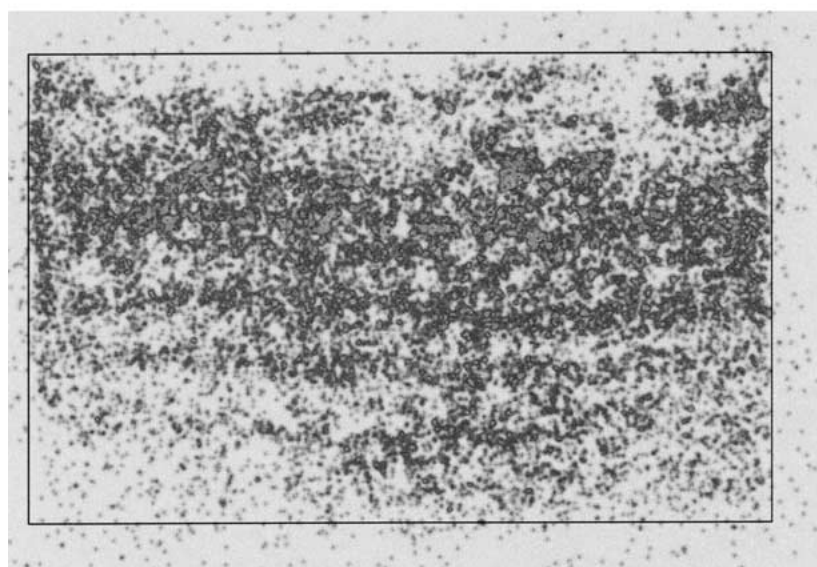


Figure 5. Two-dimensional distribution of sulfate reduction as determined with the silver foil technique (left). Mean vertical depth profiles of sulfate reduction as determined by averaging over the width of the front and back side of the incubated silver foil (right).

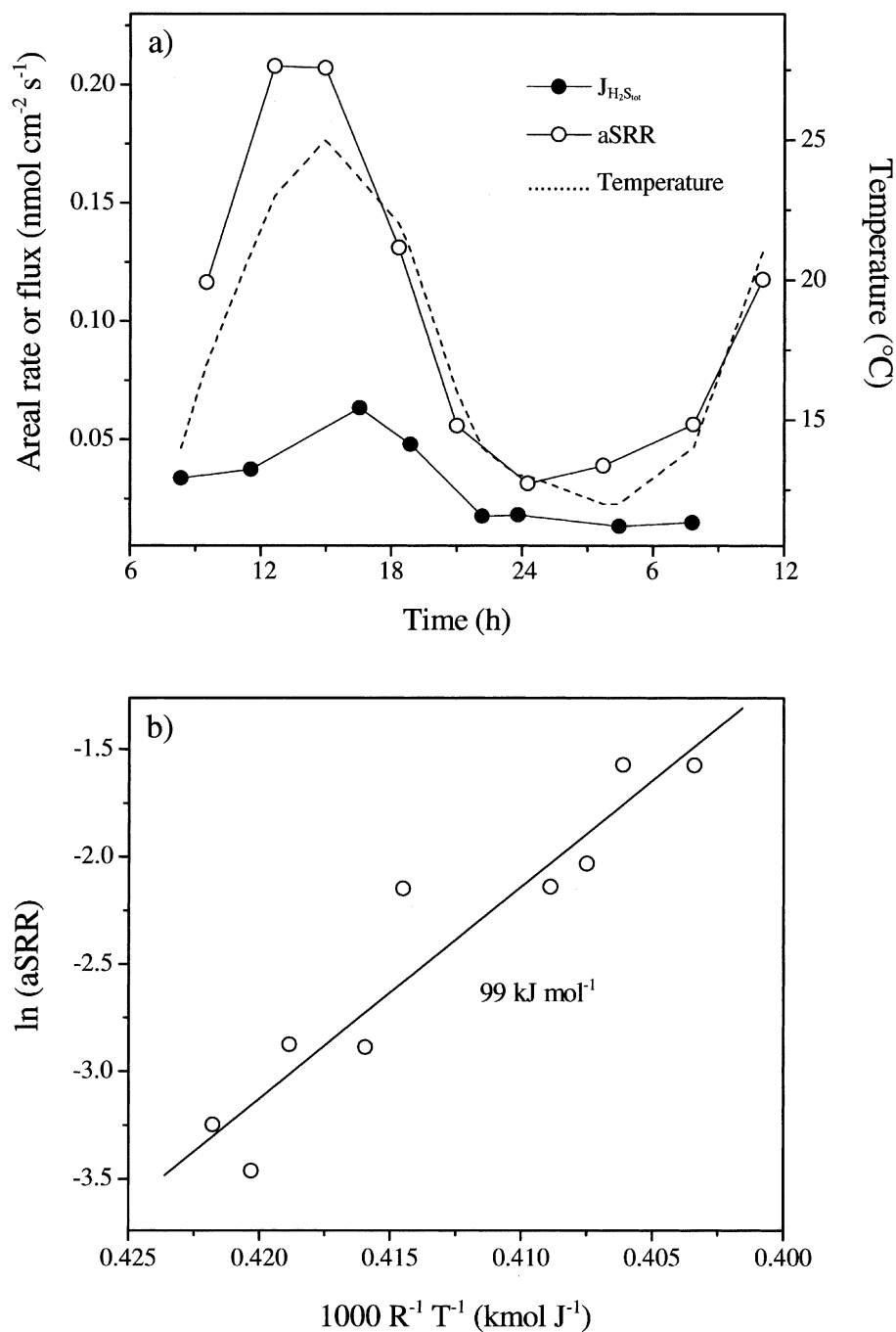


Figure 6. Areal rates of sulfate reduction (aSRR) determined by depth-integration of the data shown in Fig. 4, and sulfide fluxes ($J_{H_2S_{tot}}$) determined from the microsensor profiles shown in Fig. 2, over the diel cycle (a). The dotted line shows diel temperature variations, (b) Arrhenius plot of aSRR.

Sulfur Intermediates (Elemental Sulfur, Thiosulfate, Sulfite). Peaks of elemental sulfur (S^0), thiosulfate ($S_2O_3^{2-}$) and sulfite (SO_3^{2-}) were detected at ~ 1 – 2 mm depth during daytime (Fig. 7), indicating intense sulfide oxidation. Elemental sulfur was the dominant sulfur intermediate and high contents of 40 – $50\ \mu mol\ S^0\ cm^{-3}$ were detected in this layer (Fig. 7a). The content of S^0 in the top 6 mm of the mat increased in the morning to a maximum in the afternoon (14:57 h) and then decreased again to minimal contents in the night (Fig. 7d). This

and the localization of the S^0 peak right underneath the oxic zone (Fig. 7a) in the layer of high SRR at simultaneous low sulfide concentrations (Figs. 2A, 4) points to anoxygenic photosynthesis.

Iron (Fe(II), Fe(III), FeS, CRS). The iron content in the uppermost 6 mm of the mat was much higher than in other hypersaline *Microcoleus chthonoplastes*-dominated microbial mats (Table 1). The iron contents of mats located in river deltas along the Mediterranean coast

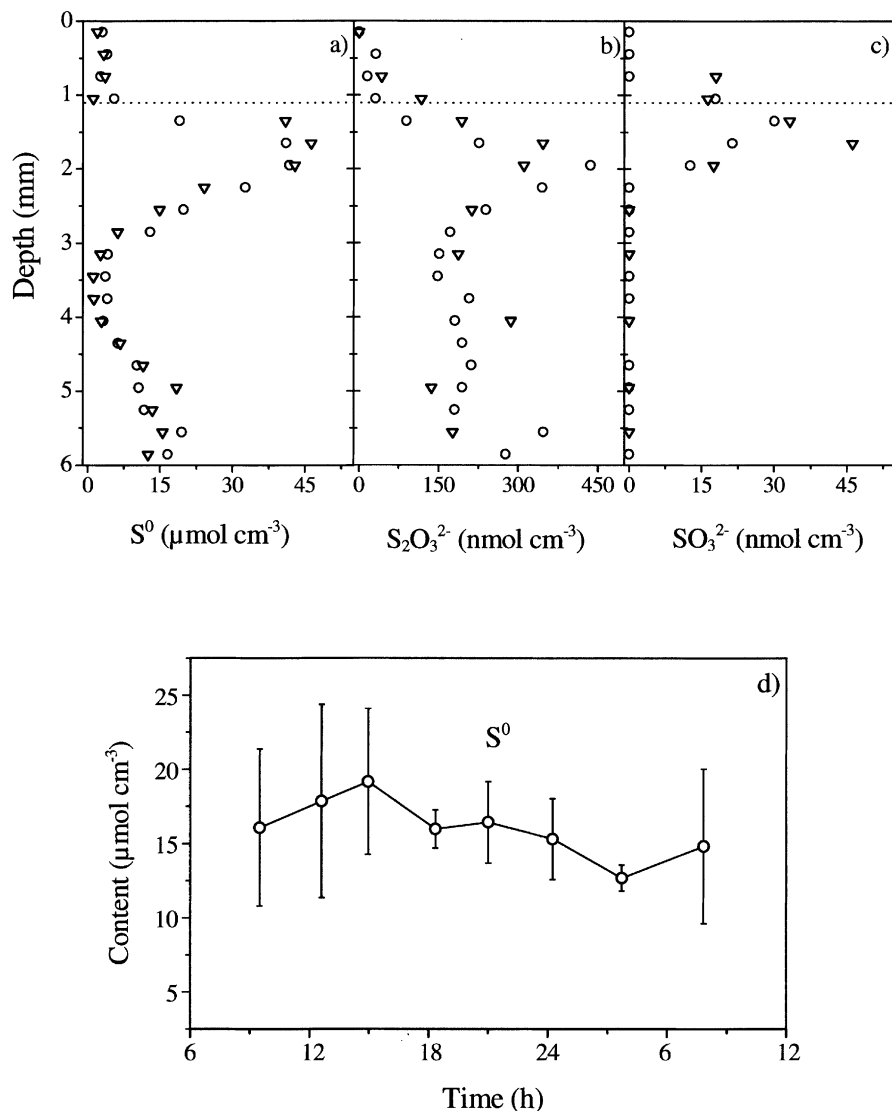


Figure 7. Depth profiles of elemental sulfur (S^0) (a), thiosulfate ($S_2O_3^{2-}$) (b), and sulfite (SO_3^{2-}) (c) at 12:37 h, as determined in two mat core samples (triangle, circle). Note different scales. The dotted line represents O_2 penetration depth at 11:32 h. (d) Mean content ($n = 4$) of S^0 in the uppermost 6 mm of the mat over the diel cycle. Error bars indicate standard deviation.

(Camargue and Ebro Delta mats) were significantly higher than the ones from the hypersaline Solar Lake, Egypt, and from evaporation ponds in Guerrero Negro, Mexico.

High contents of Fe(II) were detected in the Camargue mat below 2 mm depth both during the day and night (Fig. 8a), indicating a pronounced sulfide precipitation by iron. FeS contents amounted to $>60 \mu\text{mol cm}^{-3}$ at 4–5 mm depth, and strongly increased further at greater depths (Fig. 9a). Maximal Fe(III) contents were much lower than maximal Fe(II) contents (Fig. 8), probably due to incomplete Fe(III) extraction. Furthermore, manganese contents were low compared to the iron contents and were nearly constant with depth (Fig. 8c). However, these Mn(II) contents rather represent total manganese, because potentially present manganese oxides were rapidly reduced by Fe^{2+} during extraction.

In the uppermost 2 mm of the mat, the ratio of reduced (acid volatile) sulfur (S) to Fe(II) was <1 (Fig. 9c). In this mostly oxic and Fe(III)-rich mat layer, efficient sulfide reoxidation by O_2 , Fe(III), and anoxygenic photosynthesis prevented an accumulation of a free sulfide pool and a precipitation of FeS (Figs. 9a, c). Thus, the Fe(II) pool in that mat layer was mainly composed of other iron species than FeS.

Table 1. Iron content of the uppermost 6 mm of different hypersaline cyanobacterial mats

	$\mu\text{mol Fe cm}^{-3}$
Camargue	55.7
Ebro Delta ^a	24.2
Solar Lake	4.6
Guerrero Negro ^b	4.7

^aOnly uppermost 5.3 mm.

^bB. Thamdrup pers. comm. (iron extracted by the same procedure as in the other mats).

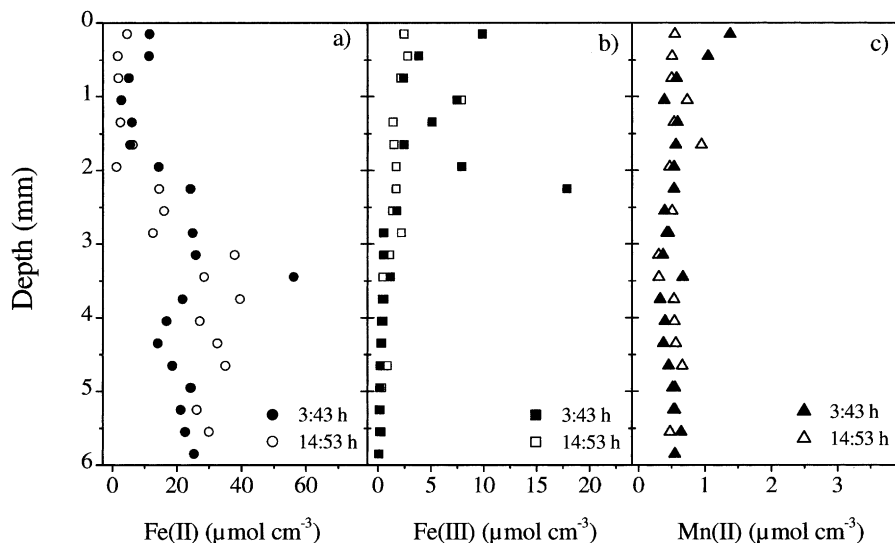


Figure 8. Average depth profiles ($n = 2\text{--}3$) of Fe(II) (a), Fe(III) (b), and Mn(II) (c) in the mat at 14:53 h (open symbols) and 3:43 h (closed symbols). Note different scales.

In the anoxic layer at 2–5 mm depth, which exhibited lower Fe(III) and highest Fe(II) contents (Figs 8a, b) at maximal sulfate reduction rates (Fig. 4), the S to Fe(II) ratio approached ~ 1 because of an almost complete precipitation of Fe(II) as FeS. In this and in deeper anoxic layers precipitation of FeS was the dominant process of sulfide removal leading to increasing FeS contents with depth. In the anoxic mat layers (2–10 mm), FeS was much more abundant than CRS (FeS₂ + S⁰) (Figs. 9a, b). Only a minor fraction of the CRS pool consisted of FeS₂ as found by subtraction of S⁰ (Fig. 7) from CRS. Pyrite formation did not increase with depth, and FeS was thus the dominant form of iron sulfide within the upper centimeter of the mat. A clear difference of 14 $\mu\text{mol cm}^{-3}$ of CRS between the day and night profile was observed at 2 mm depth (data not shown) supporting the diel dynamic of the S⁰ pool (Fig. 7d).

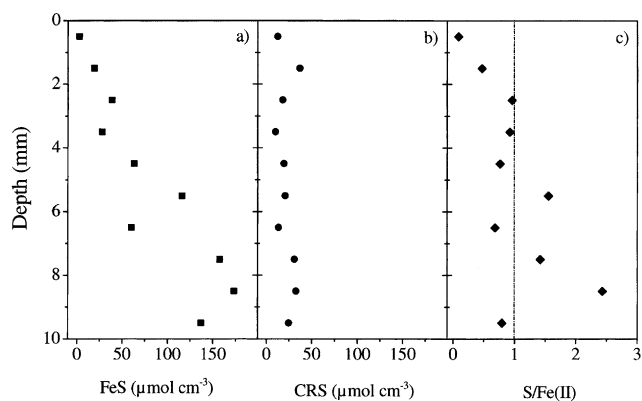


Figure 9. Average depth profiles of FeS (a) and CRS (FeS₂ + S⁰) (b) determined in two mat cores from 12:37 h and 3:43 h, respectively. (c) Ratio of acid volatile sulfur (FeS + H₂S_{tot}) to Fe(II) content, S/Fe(II).

Diel Variation of Total DIC and O₂ Fluxes. In the afternoon and around midnight, total O₂ fluxes determined by mat core incubations were approximately twice as high as the diffusive fluxes determined from measured O₂ microprofiles, whereas in the morning before sunrise both total and diffusive fluxes were more or less identical (Table 2). The DIC fluxes in the afternoon were lower than the corresponding total O₂ fluxes, whereas the opposite was observed in the night. The DIC to O₂ flux ratio was 0.75 in the afternoon and 1.83 and 1.93 during different times in the night, respectively. Assuming that 2 mol CO₂ were produced per mol sulfate reduced, sulfate reduction within the mat was the major DIC source during daytime (DIC_{SRR}) as calculated from the aSRR (Fig. 6). The bulk of the nighttime DIC fluxes out of the mat originated from sulfate reduction (64–99%), which was clearly the major process of carbon mineralization.

Discussion

Total and Diffusive Oxygen Fluxes. Oxygen fluxes across the mat–water interface were determined from microprofiles measured *in situ* (diffusive O₂ fluxes) and from core incubations (total O₂ fluxes). The major differences between diffusive and total O₂ fluxes (Table 2) were due to different flow conditions, surface topography, and microheterogeneity. The diffusive flux is mainly determined by the activity in a particular microzone and by the topography of the surrounding mat surface [29, 30]. Diffusive fluxes are generally lower than measured total fluxes [3] as a flat mat surface is assumed for the flux calculations from O₂ microprofiles, potentially underestimating the true surface area [29]. Total flux measurements over a known surface area are less sensitive to local changes of surface topography and hence give a better estimate of average mat activity. Yet, the fluxes of

Table 2. DIC and O₂ fluxes from core incubations of a mat (total fluxes) and O₂ fluxes determined from microsensors profiles (diffusive fluxes, Fig. 3) measured at different times during the diel cycle

Time (h)	Diffusive O ₂ flux (nmol cm ⁻² s ⁻¹)	Total O ₂ flux (nmol cm ⁻² s ⁻¹)	Total DIC flux (nmol cm ⁻² s ⁻¹)	Total DIC/O ₂ flux	Total DIC _{SRR} (nmol cm ⁻² s ⁻¹)	Total DIC _{SRR} (% of total DIC flux)
16:25	0.133	0.256	-0.192	0.75	0.414 ^a	216
23:32	-0.029	-0.053	0.098	1.83	0.063	64
4:14	-0.030	-0.041	0.078	1.93	0.077	99

Negative fluxes denote solute uptake, positive fluxes release from the mat. Total DIC production by sulfate reduction in the mat (DIC_{SRR}) calculated from aSRR at corresponding times (Fig. 6).

^aMeasured at 14:57 h.

O₂ across the mat–water interface are also strongly affected by the flow velocity [29, 34], as well as by the presence of microsensors [18]. Since the water flow changed during the diel cycle, the observed differences between diffusive and total fluxes were most probably mainly due to a different flow regime *in situ* and within the core. Although diffusive fluxes better reflect *in situ* rates, the advantage of core incubations is, however, that under *in situ* light and temperature conditions the total DIC flux can be determined together with the total O₂ flux, which allows correlation of oxygen cycling with the carbon cycle of the mat.

Total Oxygen and DIC Fluxes. Carbon fixation and O₂ production by oxygenic photosynthesis during daytime results in a net uptake of DIC and release of O₂ from the mat. A DIC to O₂ conversion ratio of >1 is typically found in cyanobacterial mats [3, 13] and diatom-dominated shallow-water sediments [14]. This was explained either by production of oxidized carbon in light and subsequent consumption during the night [3] or by an underestimation of net photosynthesis by the measured O₂ flux due to pronounced O₂ consumption by the oxidation of metal sulfides accumulated during darkness [13, 14].

The DIC to O₂ flux ratio <1 found in this study and the calculated DIC production by sulfate reduction (Table 2) indicate a significant CO₂ production within the mat and direct phototrophic fixation of the CO₂ produced by sulfate reduction. A close coupling between autotrophic and heterotrophic processes in hypersaline microbial mats has been reported in the literature [3, 20, 56].

Assuming that the C oxidation state of produced and mineralized organic matter is on average zero and that ammonia is the major nitrogen source, an increased internal CO₂ supply to the phototrophic community does only result in a ratio of <1 for DIC and O₂ fluxes if this internal CO₂ fixation is not accompanied by a simultaneous increase of O₂ consumption in the mat. Main CO₂-producing processes in illuminated mats are aerobic respiration and sulfate reduction. In the oxic zone, CO₂ production by both processes results in a

simultaneous and equivalent O₂ consumption; in the case of sulfate reduction due to immediate reoxidation of the produced sulfide to sulfate (2 mol O₂ consumed per mol sulfide oxidized). Sulfate reduction just underneath the oxic zone, however, could lead to diffusional DIC supply to the phototrophs without a contemporary and equivalent O₂ consumption if the produced sulfide is efficiently removed, e.g., via reactions with iron or by anoxygenic photosynthesis.

During daytime, a gap between the oxic and sulfidic zone was detected in the Camargue microbial mat (Fig. 2). In the layer just underneath the oxic zone SRR were highest, anoxygenic photosynthesis was indicated by the peak of S⁰, and Fe(II) and FeS contents were high. We speculate that sulfate reduction just underneath the oxic zone could have supplied DIC to both oxygenic and anoxygenic phototrophs and that the high iron content together with anoxygenic photosynthesis could efficiently remove the produced sulfide leading to a DIC to O₂ flux ratio <1. The proposed mechanism is new for hypersaline microbial mats and is only relevant in the presence of high iron concentrations and/or high rates of anoxygenic photosynthesis.

The determined ratio of 1.8–1.9 between nighttime DIC and O₂ fluxes (Table 2) shows that O₂ uptake rates strongly underestimate carbon mineralization during the night [3, 14], assuming that carbonate dissolution does not significantly contribute to nighttime DIC fluxes [13]. Dark O₂ consumption in hypersaline microbial mats is limited by the diffusive O₂ supply from the overlying water caused by the constraints on mass transfer imposed by the DBL [56]. A ratio of nighttime DIC to O₂ fluxes >1, as typically found in mats, could also partly be due to consumption of oxidized carbon accumulated during the day in periods of high photosynthesis [3]. It was shown in hypersaline mats that glycolate can serve as potential substrate for sulfate-reducing bacteria [17] and that aerobic heterotrophic bacteria can grow on cyanobacterial photosynthetic excretion products [26].

Sulfate Reduction. In the Camargue mats, sulfate reduction clearly dominated carbon mineralization and accounted for maximally 64–99% of the DIC released

from the mat during nighttime (Table 2). Thus, the contribution of organotrophic aerobic respiration decreased from $\sim 36\%$ of the total DIC flux at midnight to $\sim 1\%$ in the early morning before sunrise. This contribution would be even lower if Fe(III) and/or S^0 served as electron acceptors for respiration or if carbonate dissolution contributed to the DIC efflux during the night. Assuming that 1 mol DIC is produced per mol O_2 respired, aerobic respiration would account for $\sim 66\%$ and $\sim 1\%$ of the total O_2 flux (Table 2). Thus, $\sim 34\%$ to $\sim 99\%$ of the nighttime O_2 consumption rate was due to oxidation of reduced compounds such as sulfide and Fe(II)/FeS.

Our data clearly show that internal carbon cycling and especially sulfate reduction is the most important DIC source for photosynthetic CO_2 fixation (Table 2). Previous studies showed that daytime DIC production by sulfate reduction was lower than the DIC influx from the overlying water [3]. Thus, sulfate reduction plays a significant role in the Camargue microbial mats and is quantitatively more important for carbon mineralization and substrate interactions with phototrophs than hitherto found in other hypersaline mats.

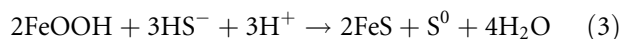
Temperature apparently played an important role in the regulation of *in situ* bacterial sulfate reduction activity in the Camargue microbial mats (Fig. 6). Sulfate reduction rates closely following daily temperature variations in hypersaline microbial mats were also found by Jørgensen [27]. However, the Q_{10} of sulfate reduction in the Camargue mat of 4 is one of the highest values found for microbial mats and saltmarsh sediments [1, 27, 49]. The strong increase of sulfate reduction during the day indicates a sufficient supply of organic carbon substrates either directly from the phototrophic community in the form of photosynthate or from fermentation in the anoxic zone. Sufficient or even excessive availability of organic carbon substrates is a prerequisite for the observed strong temperature response of SRR. Thus, our data strongly indicate that photosynthesis and sulfate reduction are tightly coupled via photosynthate and CO_2 turnover [3, 17].

Maximal rates of sulfate reduction during the day at $23^\circ C$ amounted to $0.208 \text{ nmol cm}^{-2} \text{ s}^{-1}$, which is within the upper range of rates reported for hypersaline microbial mats. Daytime sulfate reduction rates of $0.028\text{--}0.212 \text{ nmol cm}^{-2} \text{ s}^{-1}$ were found in mats from the Mexican saltern at Baja California at temperatures of $20^\circ C$ and $30^\circ C$, respectively, with lower SRR ($<0.083 \text{ nmol cm}^{-2} \text{ s}^{-1}$) being more representative for this mat [3]. Sulfate reduction rates of $0.010\text{--}0.521 \text{ nmol cm}^{-2} \text{ s}^{-1}$ were detected in gypsum crusts from the Salin-de-Giraud saltern at higher salinities [5] and of $0.038 \text{ nmol cm}^{-2} \text{ s}^{-1}$ in mats kept in a hypersaline pond [27].

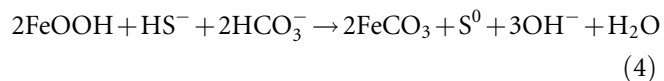
The silver foil technique revealed a horizontal lamination pattern, possibly caused by alternating organic

rich and poor layers. A small-scale heterogeneity of sulfate reduction was also observed, which may reflect an inhomogeneous distribution of suitable substrates for the SRB. A patchy distribution of photosynthesis and respiration including co-occurrence of microzones of maximum photosynthesis and respiration activity was also shown for hypersaline microbial mats, most probably as a result of tightly coupled substrate interactions between autotrophs and heterotrophs [20]. Furthermore, some SRB from hypersaline microbial mats tend to aggregate, e.g., in response to O_2 [32].

Sulfate Reduction Rates and Sulfide Fluxes. The difference between aSRR and microprofile-derived sulfide fluxes varied strongly during the diel cycle (Fig. 6a) due to various sulfide removal mechanisms. They led to relatively low sulfide concentrations at simultaneous high sulfate reduction rates (Fig. 4) and to a gap between the oxic and the sulfidic zone (Fig. 2). The large difference during the day was probably mainly caused by anoxygenic photosynthesis. Besides anoxygenic photosynthesis, also reactions of sulfide with Fe(III)-oxides in the uppermost mat layers according to



and possibly also



contributed to the observed difference between sulfate reduction rates and sulfide fluxes. Sulfide oxidation by Fe(III) was probably most significant after sunset (22:10–23:49 h) in the top $\sim 2 \text{ mm}$ (Figs. 2, 8), where Fe(III) accumulated during daytime in the former oxic zone reacted with the produced sulfide (Fig. 10). The occurrence of these reactions was also indicated by the unusual persistence of a pH peak in the surface layer from sunset until midnight and the increasing gap between the oxic and sulfidic zone when O_2 penetration decreased in that time interval (Fig. 2B).

Other processes contributing to the difference between aSRR and sulfide fluxes both during the day and night included sulfide precipitation by iron (Figs. 9, 10) and aerobic oxidation of sulfide produced in the oxic zone, where sulfate reduction activity was detected throughout the day (Figs. 4, 5).

Iron Cycling. Iron cycling mainly occurred within the uppermost $\sim 1.5 \text{ mm}$ of the mat, i.e., the oxic zone during the day (Fig. 10). In this mat layer, Fe(II) and FeS accumulated during the night and were reoxidized during sunrise and onset of oxygenic photosynthesis. Increasing irradiance and therefore increasing oxygenation of the

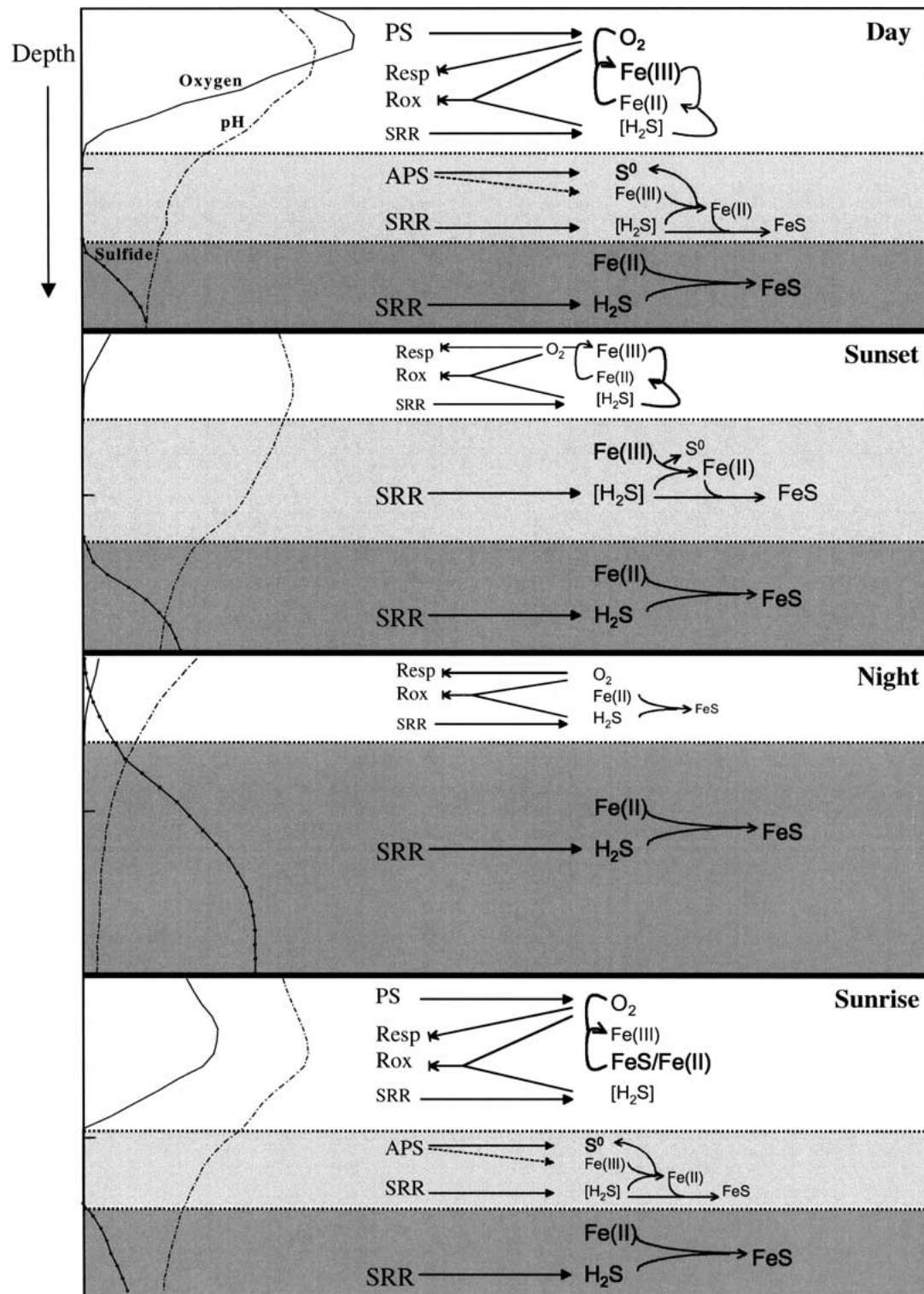


Figure 10. Scheme depicting the major biological processes and abiotic reactions in the different layers of the Camargue mat during the day, sunset, night and sunrise. Left: Schematic depth distribution of O₂, pH, and sulfide concentrations in the uppermost ~2.5 mm of the mat. Center: Major biological processes with PS denoting oxygenic photosynthesis, Resp: aerobic respiration; Rox: chemolithotrophic sulfide oxidation; SRR: sulfate reduction; and APS: anoxygenic photosynthesis. Production of a solute is indicated by → and solute consumption by ←, with a dashed arrow line indicating that the occurrence of the biological process is not certain. Microbial iron reduction and chemolithotrophic iron oxidation were omitted in the scheme, because it can only be speculated on their occurrence. Right: Abiotic reactions (→) of the different solutes. [H₂S] indicates that the produced H₂S does not accumulate because of high turnover rates.

mat during the day led to accumulation of Fe(III). Reduction of Fe(III) occurred at the same time in the oxic layer via the H_2S produced by sulfate reduction, but Fe(III) predominated due to rapid re-oxidation of the formed Fe(II). During sunset at decreasing O_2 penetration and concentration but constant depth of the upper sulfide boundary, the accumulated Fe(III) pool in this layer reacted with the produced sulfide (Eqs. 3, 4), leading to an unusual persistence of a pH peak and an increased gap between the oxic and sulfidic zone until at least midnight. After exhaustion of the Fe(III) deposits toward the end of the night, FeS and free sulfide accumulated in this layer, which was again reoxidized during sunrise.

Iron cycling could have also occurred during the day in the layer between the oxic and the sulfidic zone. However, since O_2 does not reach this depth, a prerequisite for iron cycling would be production of Fe(III) by Fe^{2+} -dependent anoxygenic photosynthesis in this layer at suitable light conditions. This Fe(III) would react immediately with the produced sulfide (Eq. 3) in this layer of high sulfate reduction activity and might have, in addition to sulfide-dependent anoxygenic photosynthesis, also contributed to the detected S^0 peak (Fig. 7). Sulfate reduction and FeS precipitation at greater depth underneath the oxic zone and the zone of anoxygenic photosynthesis led to burial and therefore buildup of a pronounced FeS and reduced sulfur pool with depth (Fig. 9).

The elevated iron contents clearly affected the biogeochemistry and especially the sulfur cycle of the Camargue microbial mat by significantly reducing the free sulfide pool at high sulfate reduction rates and by decoupling direct O_2 -sulfide interactions especially during sunset and sunrise, but also during the day together with anoxygenic photosynthesis.

Besides abiotic reactions with O_2 and sulfide, diverse direct microbial processes can be involved in iron cycling, such as anoxygenic photosynthetic oxidation of Fe(II) and FeS by purple and green phototrophic bacteria [22, 23, 51, 55]. Furthermore, it has been proposed that cyanobacteria could perform a Fe^{2+} -dependent photosynthesis [6], and Pierson et al. [43] found that Fe(II) additions stimulated photosynthetic carbon fixation in some microbial mats of iron-depositing hot springs. From our data, however, it cannot be concluded whether iron-dependent photosynthesis occurred underneath the oxic zone, since the Fe(III) produced by this process would immediately be reduced abiotically by the produced sulfide in that layer (see above and Fig. 10). Thus, both the iron and S^0 data do not allow a distinction between sulfide- and iron-dependent photosynthesis and only indicate that anoxygenic photosynthesis took place in that layer.

Aerobic microbial iron oxidation would probably be confined to the oxic-anoxic interface [10]. At the pre-

vailing pH during day- and nighttime, ranging from pH ~ 7 to 9.5, abiotic iron oxidation with O_2 could predominate, although microbial iron oxidation cannot be completely excluded. Another potential oxidant of iron is H_2O_2 [39], which can be a by-product of oxygenic photosynthesis [38]. Microbial Fe(III) reduction by different groups of bacteria [36, 52] cannot be excluded, but because of the very high sulfate reduction rates, most of the iron was probably reduced abiotically by reactions with sulfide. Thus, iron cycling was mainly controlled by chemical reactions with sulfide and O_2 , as indicated in our biogeochemical data.

The high iron contents found in the Camargue mats have to our knowledge not been found in other hypersaline microbial mats. The higher iron contents in microbial mats from river deltas (Ebro Delta, Rhône Delta) compared to mats from other sites (Table 1) point to an input of, e.g., iron-rich clay minerals during microbial mat growth. Cornée et al. [7] proposed that during strong winds and floods over the levees and dykes of the Salin-de-Giraud saltern, sand from these barriers and sediment from the river delta could be transported into the ponds. The observed lamination pattern of visible iron-rich bands in the mats indicates a noncontinuous, periodical deposition of iron.

Conclusions

A high iron content was found in the Camargue mat, which decoupled direct oxygen-sulfide interactions during most of the diel cycle. Despite of the elevated iron content, the mat biogeochemistry was mainly driven by the sulfur cycle. Anoxygenic photosynthesis contributed to sulfide turnover and sulfate reduction was the dominant mineralization process and DIC source for photosynthesis. Reactions of the produced sulfide with iron (reduction, precipitation) and partial re-oxidation of Fe(II) by photosynthetically produced O_2 dominated iron cycling in the mat. This mat system is an excellent model system to study the dynamics of iron and sulfur, as well as trace metal geochemistry, and may serve as a recent analogue to iron-rich shallow-water microbial mats as they occurred in the Proterozoic.

Acknowledgments

This study was supported by the EC (MATBIOPOL project, grant EVK3-CT-1999-00010), the Swiss National Science Foundation (J.Z., Nr. 83EU-063451), and the Danish Natural Science Research Council (M.K., contract no. 9700549). We thank the groups of Patricia Bonin (University of Marseille) and Pierre Caumette (University of Pau) for the excellent organization of the Camargue field trip in June 2001. We thank the company Salins-du-Midi at Salin-de-Giraud, France, for providing

access to the field site and laboratory facilities. Bo Thamdrup generously provided unpublished data on iron contents in Mexican microbial mats and added valuable comments which helped to improve an earlier version of the manuscript. Technical support from Lilian Salling (SDU, Odense), Armin Gieseke and Kirsten Neumann at the MPI for Marine Microbiology in Bremen is gratefully acknowledged. Anni Glud (MBL, Helsingør) is thanked for microsensor construction and technical assistance. The first and second authors contributed equally to this *in situ* study.

References

1. Abdollahi, H, Nedwell, DB (1979) Seasonal temperature as a factor influencing bacterial sulfate reduction in a saltmarsh sediment. *Microb Ecol* 5: 73–79
2. Canfield, DE, Des Marais, DJ (1991) Aerobic sulfate reduction in microbial mats. *Science* 251: 1471–1473
3. Canfield, DE, Des Marais, DJ (1993) Biogeochemical cycles of carbon, sulfur, and free oxygen in a microbial mat. *Geochim Cosmochim Acta* 57: 3971–3984
4. Carlile, MJ, Dudeney, AWL (2000) A microbial mat composed of iron bacteria. *Microbiology* 146: 2092–2093
5. Caumette, P, Matheron, R, Raymond, N, Relexans, J-C (1994) Microbial mats in the hypersaline ponds of Mediterranean salterns (Salins-de-Giraud, France). *FEMS Microbiol Ecol* 13: 273–286
6. Cohen, Y (1989) Photosynthesis in cyanobacterial mats and its relation to the sulfur cycle: a model for microbial sulfur interactions. In: Cohen, Y, Rosenberg, E (Eds.) *Microbial Mats: Physiological Ecology of Benthic Microbial Communities*, American Society for Microbiology, Washington DC, pp 22–36
7. Cornée, A, Dickman, M, Busson, G (1992) Laminated cyanobacterial mats in sediments of solar salt works: some sedimentological implications. *Sedimentology* 39: 599–612
8. Des Marais, DJ, D'Amelio, ED, Farmer, JD, Jørgensen, BB, Palmisano, AC, Pierson, BK (1992) Case study of a modern microbial mat-building community: the submerged cyanobacterial mats of Guerrero Negro, Baja California Sur, Mexico. In: Schopf, JW, Klein, C (Eds.) *The Proterozoic Biosphere: A Multidisciplinary Study*, Cambridge University Press, Cambridge, UK, pp 325–333
9. Dymond, J, Collie, RW, Watwood, ME (1989) Bacterial mats from Crater Lake, Oregon and their relationship to possible deep-lake hydrothermal venting. *Nature* 342: 637–675
10. Emerson, D, Moyer, C (1997) Isolation and characterization of novel iron-oxidizing bacteria that grow at circumneutral pH. *Appl Environ Microbiol* 63: 4784–4792
11. Emerson, D, Moyer, CL (2002) Neutrophilic Fe-oxidizing bacteria are abundant at the Loihi seamount hydrothermal vents and play a major role in Fe oxide deposition. *Appl Environ Microbiol* 68: 3085–3093
12. Emerson, D, Revsbech, NP (1994) Investigation of an iron-oxidizing microbial mat community located near Aarhus, Denmark: field studies. *Appl Environ Microbiol* 60: 4022–4031
13. Fenchel, T (1998) Artificial cyanobacterial mats: cycling of C, O, and S. *Aquat Microb Ecol* 14: 253–259
14. Fenchel, T, Glud, RN (2000) Benthic primary production and O₂-CO₂ dynamics in a shallow-water sediment: spatial and temporal heterogeneity. *Ophelia* 53: 159–171
15. Fossing, H, Jørgensen, BB (1989) Measurement of bacterial sulfate reduction in sediments: evaluation of a single-step chromium reduction method. *Biogeochemistry* 8: 205–222
16. Fourçans, A, García de Oteyza, T, Wieland, A, Solé, A, Diestra, E, van Bleijswijk, J, Grimalt, JO, Köhl, M, Esteve, I, Muyzer, G, Caumette, P, Duran, R (2003) Characterization of functional groups in a hypersaline microbial mat community (Salins-de-Giraud, Camargue, France). *FEMS Microbiol Ecol*, in press
17. Fründ, C, Cohen, Y (1992) Diurnal cycles of sulfate reduction under oxic conditions in cyanobacterial mats. *Appl Environ Microbiol* 58: 70–77
18. Glud, RN, Gundersen, JK, Revsbech, NP, Jørgensen, BB (1994) Effects on the benthic diffusive boundary layer imposed by microelectrodes. *Limnol Oceanogr* 39: 462–467
19. Glud, RN, Gundersen, JK, Revsbech, NP, Jørgensen, BB, Hüttl, M (1995) Calibration and performance of the stirred flux chamber from the benthic lander Elinor. *Deep Sea Res* 42: 1029–1042
20. Glud, RN, Köhl, M, Kohls, O, Ramsing, NB (1999) Heterogeneity of oxygen production and consumption in a photosynthetic mat. *J Phycol* 35: 270–279
21. Grasshoff, K, Ehrhardt, M, Kremling, K (1983) *Methods of Seawater Analysis*. Verlag Chemie, Weinheim
22. Heising, S, Richter, L, Ludwig, W, Schink, B (1999) *Chlorobium ferrooxidans* sp. nov., a phototrophic green sulfur bacterium that oxidizes ferrous iron in coculture with a “*Geospirillum*” sp. strain. *Arch Microbiol* 172: 116–124
23. Heising, S, Schink, B (1998) Phototrophic oxidation of ferrous iron by a *Rhodomicoccus vannielii* strain. *Microbiology* 144: 2263–2269
24. Hershey, JP, Plese, T, Millero, FJ (1988) The pK₁* for the dissociation of H₂S in various ionic media. *Geochim Cosmochim Acta* 52: 2047–2051
25. Javor, BJ (1989) *Hypersaline Environments*. Springer, Berlin
26. Jonkers, HM, Abed, RMM (2003) Identification of aerobic heterotrophic bacteria from the photic zone of a hypersaline microbial mat. *Aquat Microb Ecol* 30: 127–133
27. Jørgensen, BB (1994) Sulfate reduction and thiosulfate transformations in a cyanobacterial mat during a diel oxygen cycle. *FEMS Microbiol Ecol* 13: 303–312
28. Jørgensen, BB, Des Marais, DJ (1986) Competition for sulfide among colorless and purple sulfur bacteria in cyanobacterial mats. *FEMS Microbiol Ecol* 38: 179–186
29. Jørgensen, BB, Des Marais, DJ (1990) The diffusive boundary layer of sediments: oxygen microgradients over a microbial mat. *Limnol Oceanogr* 35: 1343–1355
30. Jørgensen, BB, Revsbech, NP (1985) Diffusive boundary layers and the oxygen uptake of sediments and detritus. *Limnol Oceanogr* 30: 111–122
31. Karl, DM, McMurty, GM, Malahoff, A, Garcia, MO (1988) Loihi Seamount: a midplate volcano with a distinctive hydrothermal system. *Nature* 335: 532–535
32. Krekeler, D, Teske, A, Cypionka, H (1998) Strategies of sulfate-reducing bacteria to escape oxygen stress in a cyanobacterial mat. *FEMS Microbiol Ecol* 25: 89–96
33. Krumbein, WE, Cohen, Y, Shilo, M (1977) Solar Lake (Sinai). 4. Stromatolitic cyanobacterial mats. *Limnol Oceanogr* 22: 635–656
34. Köhl, M, Glud, RN, Ploug, H, Ramsing, NB (1996) Microenvironmental control of photosynthesis and photosynthesis-coupled respiration in an epilithic cyanobacterial biofilm. *J Phycol* 32: 799–812
35. Köhl, M, Steuckart, C, Eickert, G, Jeroschewski, P (1998) A H₂S microsensor for profiling biofilms and sediments: application in an acidic lake sediment. *Aquat Microb Ecol* 15: 201–209
36. Lovley, DR (1991) Dissimilatory Fe(III) and Mn(IV) reduction. *Microbiol Rev* 55: 259–287
37. Lovley, DR, Phillips, EJP (1987) Rapid assay for microbially reducible ferric iron in aquatic sediments. *Appl Environ Microbiol* 53: 1536–1540

38. Luther III, GW, Glazer, BT, Hohmann, L, Popp, JI, Taillefert, M, Rozan, TF, Brendel, PJ, Theberge, SM, Nuzzio, DB (2001) Sulfur speciation monitored *in situ* with solid state gold amalgam voltammetric microelectrodes: polysulfides as a special case in sediments, microbial mats and hydrothermal vent waters. *J Env Monit* 3: 61–66
39. Millero, FJ, Sotolongo, S (1989) The oxidation of Fe(II) with H₂O₂ in seawater. *Geochim Cosmochim Acta* 53: 1867–1873
40. Mir, J, Martínez-Alonso, M, Esteve, I, Guerrero, R (1991) Vertical stratification and microbial assemblage of a microbial mat in the Ebro Delta (Spain). *FEMS Microbiol Ecol* 86: 59–68
41. Nübel, U, Garcia-Pichel, F, Clavero, E, Muyzer, G (2000) Matching molecular diversity and ecophysiology of benthic cyanobacteria and diatoms in communities along a salinity gradient. *Environ Microbiol* 2: 217–226
42. Oren, A, Köhl, M, Karsten, U (1995) An endoevaporitic microbial mat within a gypsum crust: zonation of phototrophs, photopigments, and light penetration. *Mar Ecol Prog Ser* 128: 151–159
43. Pierson, BK, Parenteau, MN, Griffin, BM (1999) Phototrophs in high-iron-concentration microbial mats: physiological ecology of phototrophs in an iron-depositing hot spring. *Appl Environ Microbiol* 65: 5474–5483
44. Revsbech, NP (1989) An oxygen microelectrode with a guard cathode. *Limnol Oceanogr* 34: 474–478
45. Revsbech, NP, Jørgensen, BB (1986) Microelectrodes: their use in microbial ecology. *Adv Microb Ecol* 9: 293–352
46. Revsbech, NP, Jørgensen, BB, Blackburn, TH, Cohen, Y (1983) Microelectrode studies of the photosynthesis and O₂, H₂S, and pH profiles of a microbial mat. *Limnol Oceanogr* 28: 1062–1074
47. Sigalevich, P, Meshorer, E, Helman, Y, Cohen, Y (2000) Transition from anaerobic to aerobic growth conditions for the sulfate-reducing bacterium *Desulfovibrio oxycloinae* results in flocculation. *Appl Environ Microbiol* 66: 5005–5012
48. Skyring, GW, Bauld, J (1990) Microbial mats in australian coastal environments. *Adv Microb Ecol* 11: 461–498
49. Skyring, GW, Chambers, LA, Bauld, J (1983) Sulfate reduction in sediments colonized by cyanobacteria, Spencer Gulf, South Australia. *Aust J Mar Freshwat Res* 34: 359–374
50. Stal, LJ (2000) Cyanobacterial mats and stromatolites. In: Whittton, BA, Potts, M (Eds.) *The Ecology of Cyanobacteria*, Kluwer, Dordrecht, pp 61–120
51. Straub, KL, Rainey, FA, Widdel, F (1999) *Rhodovulum iodosum* sp. nov. and *Rhodovulum robiginosum* sp. nov., two new marine phototrophic ferrous-iron-oxidizing purple bacteria. *Int J Syst Bacteriol* 49: 729–735
52. Thamdrup, B (2000) Bacterial manganese and iron reduction in aquatic sediments. *Adv Microb Ecol* 16: 41–84
53. Thamdrup, B, Fossing, H, Jørgensen, BB (1994) Manganese, iron, and sulfur cycling in a coastal marine sediment, Aarhus Bay, Denmark. *Geochim Cosmochim Acta* 58: 5115–5129
54. Visscher, PT, Reid, RP, Bebout, BM (2000) Microscale observations of sulfate reduction: correlation of microbial activity with lithified micritic laminae in modern marine stromatolites. *Geology* 28: 919–922
55. Widdel, F, Schnell, S, Heising, S, Ehrenreich, A, Assmus, B, Schink, B (1993) Ferrous iron oxidation by anoxygenic phototrophic bacteria. *Nature* 362: 834–836
56. Wieland, A, Köhl, M (2000) Irradiance and temperature regulation of oxygenic photosynthesis and O₂ consumption in a hypersaline cyanobacterial mat (Solar Lake, Egypt). *Mar Biol* 137: 71–85
57. Wieland, A, Köhl, M (2000) Short-term temperature effects on oxygen and sulfide cycling in a hypersaline cyanobacterial mat (Solar Lake, Egypt). *Mar Ecol Prog Ser* 196: 87–102
58. Zopf, J, Ferdelman, TG, Jørgensen, BB, Teske, A, Thamdrup, B (2001) Influence of water column dynamics on sulfide oxidation and other major biogeochemical processes in the chemocline of Mariager Fjord (Denmark). *Mar Chem* 74: 29–51